Khairul, M. A.; Alam, M; Doroodchi, Elham; Azizian, Reza; Moghtaderi, Behdad; 'Thermal performance analysis of tunable magnetite nanofluids for an energy system.' Published in *Applied Thermal Engineering* Vol. 126, Issue November 2017, p. 822-833 (2017)

Available from: http://dx.doi.org/10.1016/j.applthermaleng.2017.07.214

Thermal performance analysis of tunable magnetite nanofluids for an energy system

M.A. Khairul[1], Elham Doroodchi[2], Reza Azizian[3], Behdad Moghtaderi[1,]*

[1]Priority Research Centre for Frontier Energy Technologies and Utilisation, Chemical Engineering, Faculty of Engineering and Built Environment, The University of Newcastle, Callaghan, NSW 2308, Australia.

[2]Center for Advanced Particle Processing, Chemical Engineering, Faculty of Engineering and Built Environment, The University of Newcastle, Callaghan, NSW 2308, Australia.

[3]Advanced Thermal Solution Inc., 89-27 Access Road, Norwood 02062, MA, USA.

Abstract

This study is based on the effect of external magnetic field on heat transfer performance and pumping power of Fe_3O_4/DI-water nanofluid is experimentally investigated under both laminar and turbulent flow regimes. The magnetite ferrofluids with 0.25% and 0.50% of weight fractions are prepared by a chemical precipitating method using ammonium hydroxide reagent for maximising the stabilisation. The experiments were conducted at various mass flow rates with two different external magnets arrangements and input powers. The result shows that the enhancement in local heat coefficient was more pronounced by introducing more magnets on the tube of the test section, especially in the turbulent flow regime. The heat transfer coefficient improves with an increase in Reynolds number as well. In addition, the effect of the magnetic field was not significant on the increment of pressure loss. Therefore, the highest performance index and lowest exergy loss were found for external magnets configurations at 0.25 wt% of nanofluids. The rise in heat transfer is assumed to be an accumulation of nanoparticles near the ring magnets, which may lead to a local thermal conductivity improvement. This aggregation formation enhancing the momentum and energy transfer in the fluid flow.

* Corresponding author: Tel: +61 2 4033-9062, Fax: +61 2 4033-9095
Email: Behdad.Moghtaderi@newcastle.edu.au (Attn: Professor Behdad Moghtaderi)

Keywords: heat transfer performance; magnetite ferrofluids; magnetic field; performance index; exergy loss

Nomenclature

c_p	specific heat capacity (*J/kg K*)		Greek symbols	
C	heat capacity rate (*W/K*)		φ	particles volume fraction
D	tube diameter (*m*)		ρ	density (kg/m^3)
E_{loss}	exergy loss (*J*)		μ	viscosity ($N\ s/m^2$)
f	friction factor		β	thermal expansion coefficient (K^{-1})
Gr	Grashof number		η	performance index
g	acceleration of gravity (m/s^2)		Subscripts	
h	heat transfer coefficient ($W/m^2\ K$)		b	bulk
k	thermal conductivity (*W/m.K*)		bf	base fluid
L	length of the test section (*m*)		e	environment
$\dot{m}$	mass flow rate (*kg/s*)		i	inner
Nu	Nusselt number		in	input
Pr	Prandtl number		lam	laminar flow
ΔP	pressure drop (*Pa*)		nf	nanofluids
P_p	pumping power (*W*)		np	nanoparticles
q''	heat flux based on thermal power (W/m^2)		o	outer
Q	thermal power (*W*)		out	output
Re	Reynolds number		w	wall
S	tube circumference (*m*)		x	local
T	temperature (*K*)		$trans$	transitional flow
v	velocity (*m/s*)		$turb$	turbulent flow
x	distance from the entrance of the tube (*m*)			
z^+	dimensionless distance			

1. Introduction

Recent technological developments in the fields of thermal and electronics systems are associated to the rising demand for advanced heat transfer systems with greater thermal efficiencies. Therefore, several studies have been done on enhancement of heat transfer techniques by utilising active as well as passive methods. Active method involves mechanical agitation, rotation and vibration, but an external source of energy is needed in this technique. Whereas, passive method is dealing with the advancement of surface geometry and thermal properties of the fluids. Nanofluid is one of the noticeable passive methods that has potential heat transfer augmentation properties, many scientists' center of attention in recent years [1].

Several studies have been focused on Magnetic nanofluids (MNFs) [2-7]. MNFs are the mixture of base fluid (non-magnetic) and magnetic nanoparticles coated with some sorts of surfactants or reagents such as oleic acid, ammonium hydroxide to get a stable solid-fluid mixture [8, 9]. Usually magnetic nanoparticles are prepared in different sizes and morphologies from ferromagnetic materials such as nickel, iron, cobalt, and ferrimagnetic materials' oxides such as spinel-type ferrites and magnetite etc. These types of nanofluids not only possess the improvement in thermal properties but also exhibit the magnetic properties like other magnetic materials. Such unique feature of nanofluid is associated to control the heat transfer and movement of particles by using the external magnetic field with various orientations and strengths. These fluids have a potentiality to apply in different fields such as electronics cooling, bioengineering, heat exchangers, thermal engineering, energy harvesters and so on [2, 10, 11]. Investigations on magnetic nanofluids in the presence and absence of magnetic fields were demonstrated in different studies [12-19], and concluded that the thermo-physical properties of magnetite nanofluids are affected by various parameters such as magnetic fields orientations as well as strengths, nanoparticle weight concertation, properties of base-fluid, chemical composition of nanoparticles, particle size, working temperature, type of surfactant coating on the particles, and so forth.

Lajvardi et al. [20] reported the temperature profile and heat transfer coefficient of a magnetite nanofluid under different external magnetic field intensities in the laminar flow regime. Results showed that the heat transfer coefficient of the magnetite nanofluid was similar compare to base fluid in the absence of an external magnetic field. Moreover, it showed a reduction in the wall temperature profile as well as an increase in the heat transfer coefficient in the presence of an external magnetic field, and this enhancement was higher at higher external magnetic field intensities. They also studied the effect of magnet position and different heat fluxes as well. As the distance between the magnets (coils) was close, the effect of magnetic field on heat transfer enhancement was much more considerable. Goharkhah et al. [21, 22] studied the influence of constant and alternating magnetic field on convective heat transfer characteristics of magnetite nanofluid in laminar flow area. Results showed that the magnetite ferrofluid improve maximum 13.5% convective heat transfer compare to DI-water in the absence of a magnetic field. Whereas, the enhancement climbs up to 18.9% and 31.4% in the application of constant and alternating magnetic field, respectively. The effect of magnetic field on convective heat transfer of Fe_3O_4 nanofluids in laminar flow was examined by Azizian et al. [23]. A noticeable improvement in the local heat transfer coefficient was observed in high Reynolds number, and the enhancement in heat transfer was also a function of magnetic field strength and gradient. Moreover, they concluded that the effect of the magnetic field on the pressure drop was not significant.

Most of the experimental works have been done on conventional metal oxide nanofluids (TiO_2, SiO_2, ZnO, CuO, Al_2O_3) and a very small number of attentions have been paid on magnetite ferrofluids though it has more tunable nature compare to conventional nanofluids [24]. A few researches have been done on magnetic nanofluids in the laminar flow condition and magnetic field generated by using different numbers of electromagnets [20, 21, 25]. More specifically, the effect of magnetic field on heat transfer performance of magnetite nanofluids using permanent magnets in laminar, transitional and turbulent flow regimes are very limited in the current literature.

Thus, the scope of the present study is to investigate the heat transfer performance in terms of heat transfer coefficient, friction factor, pumping power, exergy loss and performance index of Fe_3O_4/DI-water nanofluids with two different nanoparticle weight concentrations (0.25 wt% and 0.50 wt%) at laminar, turbulent and transitional flow regions, and compare their exergy loss and performance index in the presence and absence of magnetic field. Exergy is defined as the maximum available work in a substance during a process that brings the system back to equilibrium with a heat reservoir. Exergy is that portion of energy that can transform to another form of energy. Analysis of exergy is necessary for improving the fluids' performance index and minimising losses, because it quantifies the location, type, and magnitudes of waste and losses [26, 27].

2. Experimental procedure and validation

2.1. Nanofluid preparation and properties

A nanofluids' stability is one of the important factors in nanofluids research. A couple of methods have been suggested to attain stable nanofluids, such as chemical or physical treatment. These treatments may involve the modification of the surface of dispersed nanoparticles, addition of extra surfactant, or enforcing strong forces on the agglomerated nanoparticles. Applying a polymer coating on magnetite nanoparticles is one of the best ways to make stable nanoparticles and avoid their transformation into maghemite [28]. In this study, a polymer coating was employed to enhance the magnetite nanoparticles stability as a result of its electrostatic and steric (electrosteric) stabilisation. It is important to control both the cluster and primary particle size of magnetite particles in order to obtain an optimum nanoparticle.

In this study, Fe_3O_4/DI-water nanofluid with 0.25% to 0.50% of particle weight concentrations have been used. The nanofluids was prepared using the one-step chemical precipitation method [28]. A reagent, ammonium hydroxide, was used to stabilise the magnetite ferrofluids at a lowest dosing rate (i.e. 5 ml/min). Because, the lowest viscosity (at any shear rate from 5 to 1050 1/s) and highest thermal conductivity values were obtained at the lowermost value of ammonia reagent dosing rate for ferrofluids according to our previous study [28]. The synthesised nanofluids were found to be very stable, and did not show any visual signs of sedimentation for more than 2 months. The properties of Fe_3O_4 nanoparticle and DI-water are shown in Table 1.

Table 1. Properties of DI-water and Fe_3O_4 nanoparticle at $T = 298\ K$ [23]

Thermophysical properties	**DI-water**	**Fe_3O_4**
Density, $\rho\,(kg/m^3)$	997	5180
Specific heat, $c_p\,(J/kg.K)$	4180	670
Viscosity, $\mu\,(Ns/m^2)$	0.0009 ± 0.0000078	-
Thermal conductivity, $k\,(W/m.K)$	0.6 ± 0.012	80

The thermophysical properties of magnetite ferrofluids were considered at a constant temperature of 298 K. The nanofluids thermophysical properties, such as density, specific heat and viscosity have been calculated by applying Eqs. (1) to (3) [29].

Density of nanofluids,

$$\rho_{nf} = (1-\varphi)\rho_{bf} + \varphi\rho_{np} \tag{1}$$

Nanofluids' specific heat,

$$c_{p,nf} = \frac{(1-\varphi)(\rho c_p)_{bf} + \varphi(\rho c_p)_{np}}{\rho_{nf}} \tag{2}$$

Viscosity of nanofluids,

$$\mu_{nf} = (1+2.5\varphi)\times\mu_{bf} \tag{3}$$

Thermal conductivity of nanofluids is obtained from Yu and Choi [30] equation:

$$k_{nf} = \frac{k_{np} + 2k_{bf} + 2(k_{np} - k_{bf})(1+\beta)^3\varphi}{k_{np} + 2k_{bf} - (k_{np} - k_{bf})(1+\beta)^3\varphi} k_{bf} \tag{4}$$

where, β denotes the ratio of the nanolayer thickness to the original particle radius. To calculate the value of thermal conductivity, it is assumed that the Fe_3O_4 nanoparticles are spherical and the value of β is 0.1 [31].

2.2. Experimental set-up

Fig. 1 presents a schematic diagram and actual picture of the experimental setup used in this study [32]. The closed-loop flow system was installed with a flow meter, miniature gear pump, coil heat exchanger, pressure transmitter, DC power supply and thermocouples. The test section in the experimental rig consisted of a stainless-steel tube of an outer diameter of 6.35 mm, inner diameter of 4.57 mm, and a length of 1 m. Eleven T-type thermocouples with bare wire configuration were placed evenly along the outer wall of the tubing to measure the wall temperature of the test section. Two T-type thermocouples with a MIMS (mineral insulated metal sheathed) configuration were used to measure the bulk inlet and outlet temperatures of the fluid, rather than the temperature of the test section directly, therefore, it will avoid any influence that may occur across the test section due to heat flux. The thermocouples were calibrated with a maximum standard deviation was 0.5 ºC (Appendix A).

A heat flux was supplied throughout the experimental test section by employing a SPV-1500 single output power supply with a rated power of 1500 W, current range of 0 to 125 A and DC output voltage is 12 V. The load regulation of the output power supply was ±0.5%. The copper electrode blocks were used to provide power into the test section, which can deliver resistive heating. Ceramic fibre insulation, 12.5 mm in thickness, was applied across the test section to minimise heat loss.

For each run, the heat transfer fluid either a nanofluid or DI-water was poured into the stainless-steel pipe through the storage tank. A miniature gear pump (12 Volt DC) was utilised to circulate the working fluid at a constant flow rate in the closed-loop flow system. The volumetric flow rate of the working fluid was measured using an ultrasonic flow meter (Cynergy- UF08B) with a maximum flow rate of 8 L/min. The accuracies of the flow meter are 5% and 3% of the reading at flow rates 0.1-0.4 L/min and 0.4-8 L/min, respectively, and the response time is better than 0.1s.

The pressure drop across the test section was measured using a high precision differential pressure transmitter (Rosemount® 3051CD) with a reference accuracy of 0.004% of span, which was calibrated from 0 to 30 kPa. The pressure transmitter was connected at the inlet and outlet of the test section as shown in Fig. 1. A coil heat exchanger was used to cool down the working fluid. Two stainless steel Swagelok ball valves were used to collect the working fluids after each run, and they permit the system to be cleaned and flushed easily. The volume of the experimental setup as well as the storage tank kept to a minimum to minimise the nanofluids requirement because of its high price and long preparation time.

The thermocouples, ultrasonic flow meter, pressure transmitter and power supply instruments were connected to a data acquisition system to carry out the measurement, and the data acquisition system was interfaced with a computer by using a NI PCI-6251 board. A NI 9214 16-channel high-accuracy thermocouple module (National Instrument, UK) was employed for the measurement of temperature at high accuracy. 'Labview' software was used for the experimental system configuration as well as control.

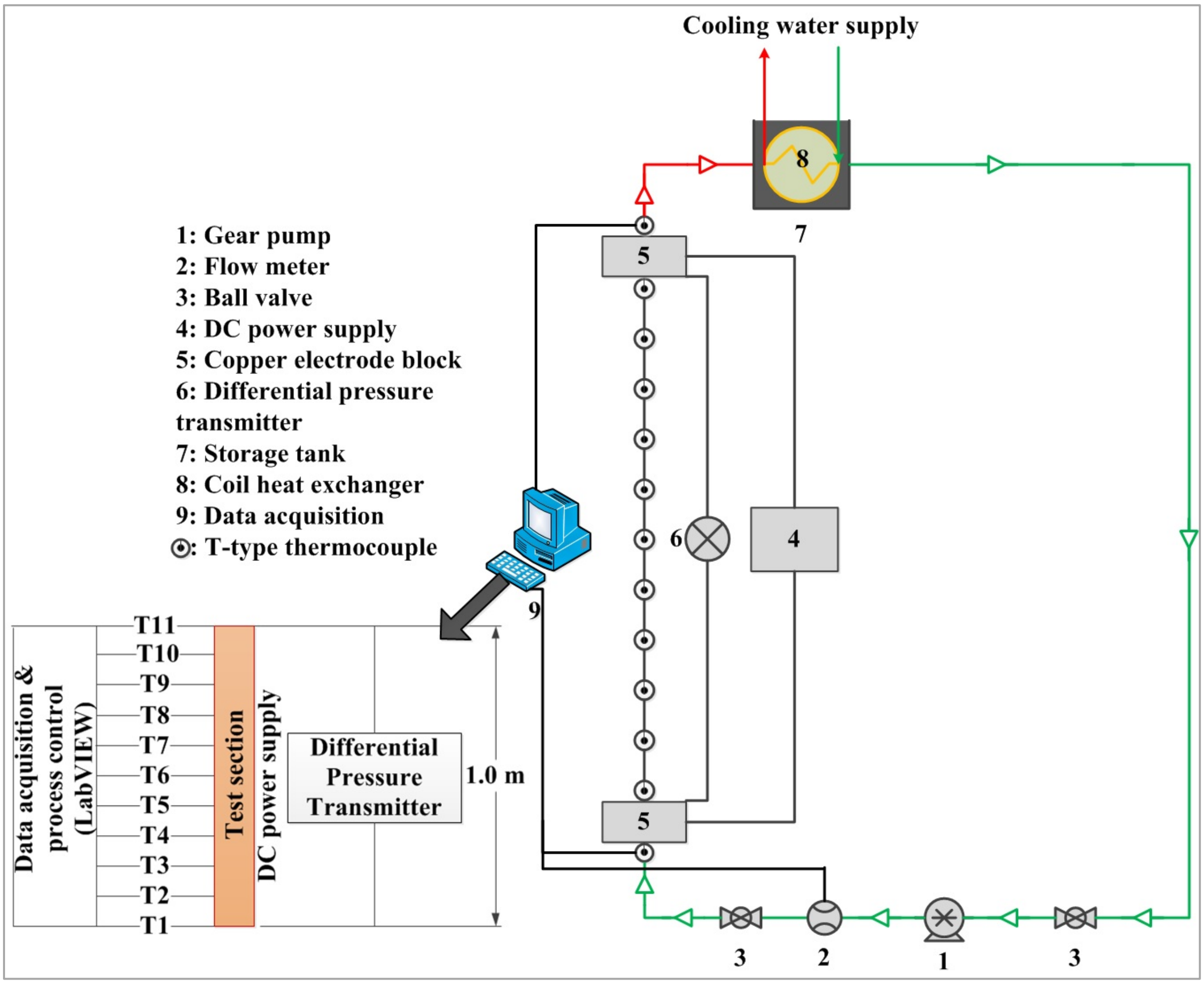

(a)

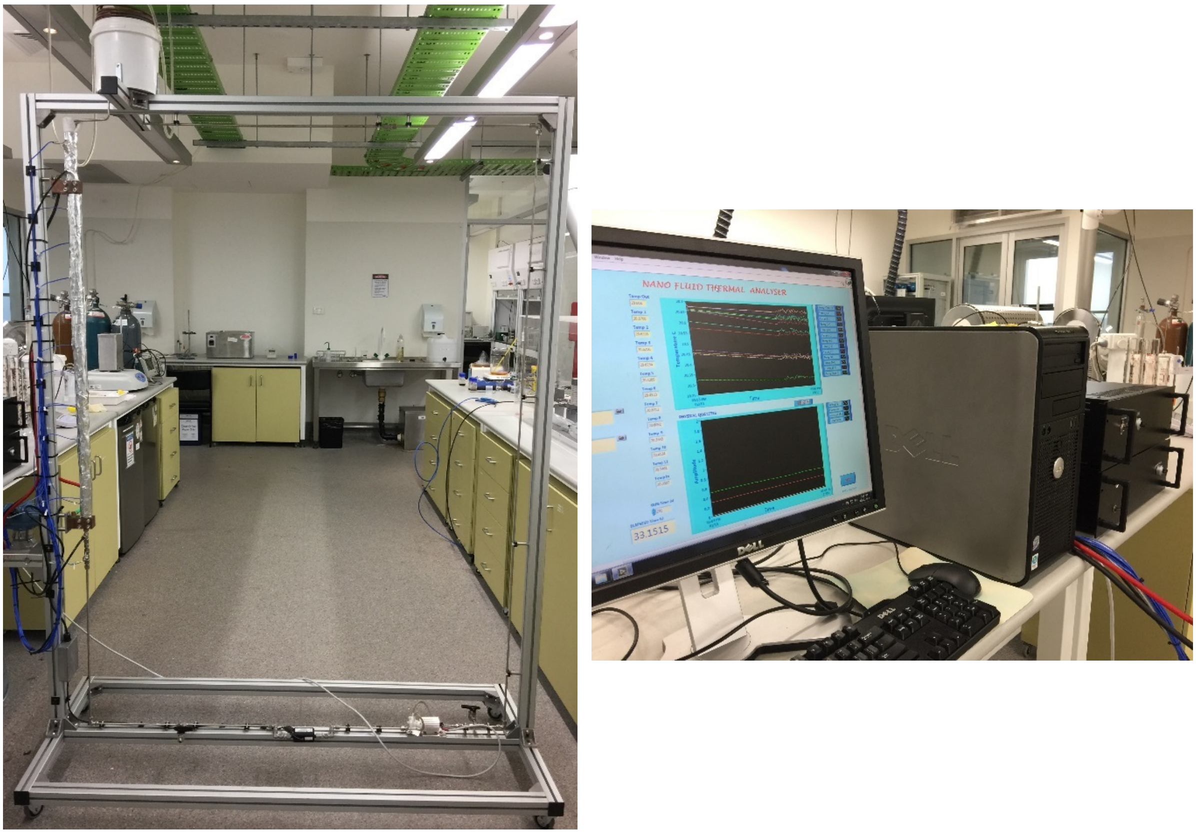

(b)

Fig. 1. An experimental set-up (a) schematic representation, (b) actual picture

In this study, the magnetic flux density was changed by varying the orientations of the permanent magnets in terms of the number of magnets and their configurations along height of the test section. Fig. 2 shows the schematic diagram of the external neodymium ring magnets configurations on the tube of the test section for two different cases. For the first case, total eight neodymium ring magnets were used across the test section, each two magnets were placed among the thermocouples T6, T7, T8, T9, T10, and the magnets were positioned among the thermocouples T2, T3, T4 as well as T6, T7, T8, T9 for another configuration.

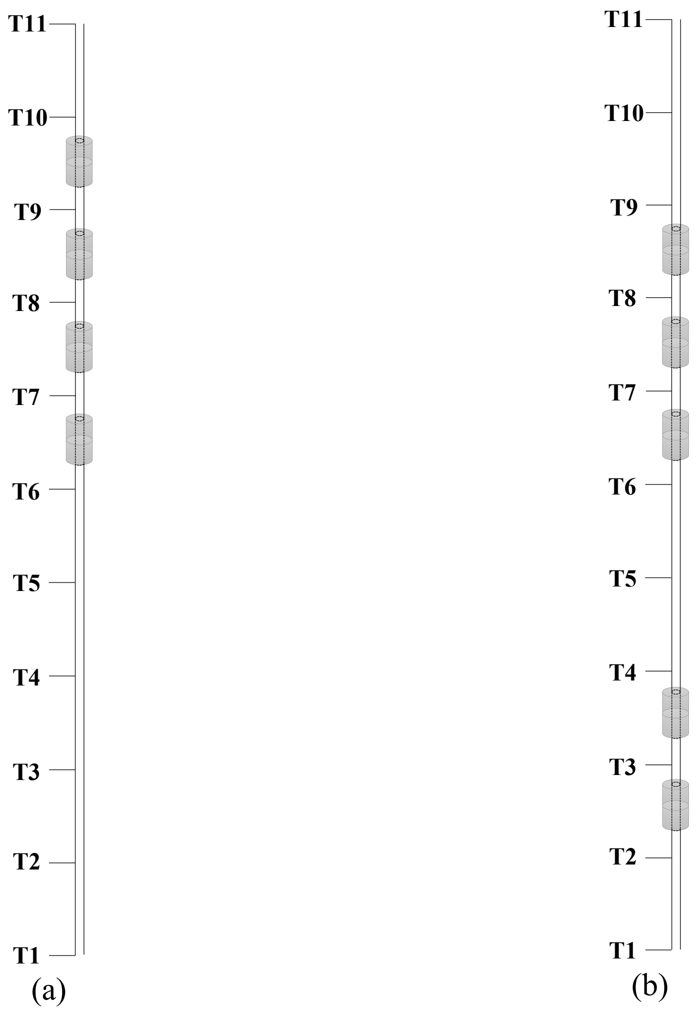

Fig. 2. Schematic diagram of ring magnets configuration (a) case 1, (b) case 2

It is very important to reach steady state conditions before taking the first data point, thus, the experimental rig was allowed to run for at least one hour at the beginning of each run. This was necessary due to the thermal inertia of the system being fairly slow initially. Steady state conditions were said to be achieved when no significant variations in the mass flow rate, temperature, and pressure drop were observed. Once the experimental system achieved steady state conditions, data acquisition at the desired mass flow rate was easier as fluctuations in the system has subsided. It was very difficult to achieve the steady state conditions in the transitional regime because of the continuous variation in pressure, mass flow rate and temperature of the working fluid. But, the results were recorded as soon as the variation in the data was repeated periodically. The experiments were conducted from larger to smaller mass flow rate to minimise the stored residual heat in the insulation, which may have an effect on the following data point. The experiments were carried out over a few days and repeated three times, each of the data points was the average of 300 readings, which was captured by using a data acquisition system. Moreover, the experiments were conducted with DI-water in the presence of magnetic field and confirm that the permanent magnets did not have any influence over the thermocouples readings.

A series of experiments has been done using Fe_3O_4/DI-water nanofluids at different flow regimes including laminar, transitional and turbulent flow with 0.25 wt% and 0.50 wt% of nanoparticle under two different orientations of permanent magnets. The effect of the magnetic field on heat transfer performance of ferrofluid in terms of local heat transfer coefficient, friction factor, exergy loss as well as performance index of ferrofluids is studied. Table 2 shows the specifications of Neodymium ring magnet utilised in this analysis.

Table 2. Neodymium (NdFeB) ring magnet specifications

Grade	N38
Maximum operating temperature	80 ºC
Surface field	550 mT
Residual flux density (Br_{max})	1300 mT
Maximum energy product (BH_{max})	40 MGOe
Style	Rare earth ring magnet
Coating	Nickel (NiCuNi)
Dimensions	Outside diameter: 22 mm Inside diameter: 7 mm Thickness: 25 mm 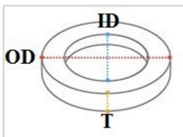
Direction of the magnetisation	Axially magnetised through the 25 mm
Tolerance	+/-0.05 mm
Weight	69 g

Given by the supplier

2.3. Experimental data analysis

The local convective heat transfer coefficient (h_x) was estimated using the following expression [23];

$$h_x = \frac{q''}{(T_{w,i} - T_b)_x} \tag{5}$$

where, q'' is the heat flux based on thermal power, L and D_i are the length and inner diameter of the test section, accordingly. $T_{w,i}$ and T_b are the inner wall and bulk temperatures of the test section, respectively at the axial location. The inside wall temperature (as shown in Eq. 6) was calculated based on the analytical solution of the conduction equation, which involves the measured external wall temperature of the test section as the boundary condition and the temperature dependent thermal resistance of stainless steel.

$$T_{w,i} = T_{w,o} - \frac{Q}{2\pi k_w L}\left[\frac{D_o^2}{\left(D_o^2 - D_i^2\right)}\log\left(\frac{D_o}{D_i} - 0.5\right)\right] \tag{6}$$

In Eq. (6), Q represents the thermal power derived from bulk outlet and inlet temperature variation of the working fluid, D_o is the outer diameter, and k_w represents the thermal conductivity of stainless steel, and it is found from a linear curve fit of data found in the ASM Handbook [33], the resulting linear fit for k_w as a function of temperature is given by the following function,

$$k_w(T) = 0.0127 \times T + 13.23188 \tag{7}$$

The fluid local bulk temperature is interpolated using the Eq. (8) as,

$$T_b(x) = \frac{q'' S}{\dot{m} c_p} x + T_{b,in} \tag{8}$$

where, S is the surface perimeter ($S = \pi D_i$ for a circular tube), $\dot{m}$ is the mass flow rate, c_p is the specific heat, x represents the axial distance from the entrance of the test section, and the fluid bulk inlet temperature is $T_{b,in}$.

Then, the local Nusselt number was evaluated by using the local convective heat transfer coefficient (h_x),

$$Nu_x = \frac{h_x D_i}{k_x} \tag{9}$$

The dimensionless Reynolds number and Prandtl number can be estimated by using Eqs. (10) and (11),

$$\text{Reynolds number, } \mathrm{Re} = \frac{4\dot{m}}{\pi \mu D_i} \tag{10}$$

$$\text{Mass flow rate } (\dot{m}) = \text{volume flow rate} \times \text{density}$$

$$\text{Prandtl number, } \mathrm{Pr} = \frac{c_p \mu}{k} \tag{11}$$

The value of pressure drop was required to estimate the Darcy-Weisbach friction factor:

$$f = \frac{2\,\Delta P.D_i}{L.\rho.v^2} \tag{12}$$

Then Eq. (12) was modified to;

$$f = \frac{\Delta P.\rho.\pi^2.D_i^5}{8\,L.\dot{m}^2} \tag{13}$$

The pressure drop was found from the measurement of the differential pressure transmitter. The required pumping power (P_p) of the fluid through the test section was calculated with Eq. (14).

$$P_p = \frac{\dot{m}}{\rho} \Delta P \tag{14}$$

Exergy loss refers to irreversible losses that occur outside the control volume. It is a loss in work availability. In contrast, exergy destruction refers to irreversible losses within the control volume [34]. Exergy losses can be minimised by reducing the temperature difference of heat transport [35]. The rate of exergy loss is calculated by assuming there is no work or heat transfer between the system and surroundings. Exergy loss for a steady state nanofluid cooling system can be expressed by Eq. (15),

$$E_{loss} = T_e \left[C \ln\left(\frac{T_{out}}{T_{in}} \right) \right] \tag{15}$$

Exergy loss caused by a reduction in fluid pressure can be neglected for liquids, because they are incompressible [36]. The environmental temperature (T_e) is assumed to be the same as the fluids' inlet temperature. The heat capacity rate (C) can be calculated by using Eq (16).

$$C = c_p \, \dot{m} \tag{16}$$

Heat transfer enhancement using nanoparticle involves rise in friction factor and pressure drop. The assessment of enhancement in heat transfer and pressure drop in the same time a term known as performance index (η) is introduced in Eq. (17), to determine the performance of a system [37].

$$\eta = \frac{h_{nf} / h_{bf}}{\Delta P_{nf} / \Delta P_{bf}} \tag{17}$$

2.4. Validation

Firstly, the results for DI-water was utilised to validate the experimental set up, because there are no other results or data points available in the existing literature for Fe_3O_4/DI-water nanofluids at the same experimental conditions. Then, the experimental result is compared with the following equations.

Ghajar and Tam [38] proposed correlations for Nusselt number in the laminar and turbulent flow regimes;

$$Nu_{lam} = 1.24\left[\left(\mathrm{Re}\,\mathrm{Pr}\,\frac{D_i}{x}\right) + 0.025\,(Gr\,\mathrm{Pr})^{0.75}\right]^{\frac{1}{3}}\left(\frac{\mu_b}{\mu_w}\right)^{0.14} \tag{18}$$

$$\text{Local bulk Grashof number, } Gr = \frac{g\beta\rho^2 D_i^3 (T_{wi} - T_b)}{\mu^2} \tag{19}$$

$$Nu_{turb} = 0.023\,\mathrm{Re}^{0.8}\,\mathrm{Pr}^{0.385}\left(\frac{x}{D_i}\right)^{-0.0054}\left(\frac{\mu_b}{\mu_w}\right)^{0.14} \tag{20}$$

Ghajar and Tam [38] formulated an equation for the transitional flow, and in this study, it was modified for a developing length inlet condition;

$$Nu_{trans} = Nu_{lam} + \left[e^{\frac{\mathrm{Re}_{trans} - \mathrm{Re}}{65}} + Nu_{turb}^{-0.935}\right]^{-0.935} \tag{21}$$

The local theoretical Nusselt numbers are also estimated by applying the Shah [39] and Gnielinski equations [40] for laminar and turbulent flow regimes, respectively and compared with the experimental results of DI-water. Shah equation (Eq. 22) is a curve fitting to the complex analytical solution of the local Nusselt number under the constant heat flux boundary condition as well as laminar flow regime [39];

$$Nu = \begin{cases} 1.302\left(\dfrac{z^+}{2}\right)^{-1/3} - 0.5 & z^+ \le 0.003 \\ 4.364 + 0.263\left(\dfrac{z^+}{2}\right)^{-0.506} e^{-41(z^+/2)} & z^+ > 0.003 \end{cases} \tag{22}$$

where z^+ is a dimensionless distance expressed as;

$$z^+ = \frac{2(x/D_i)}{\mathrm{Re}\,\mathrm{Pr}} \tag{23}$$

In Eq. (23), x is the vertical distance between the entrance of the tube and the location of the thermocouples.

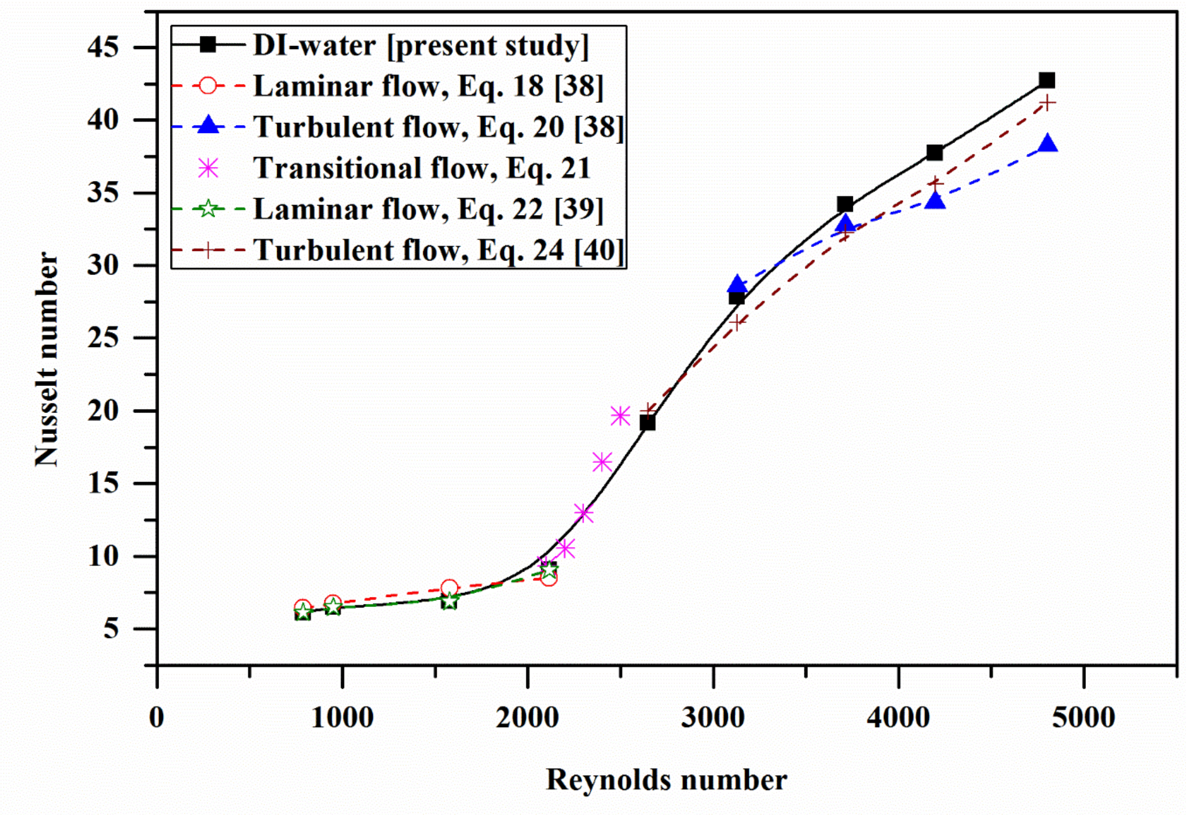

Fig. 3. Nusselt number versus Reynolds number results compared with the existing correlations for DI-water at $x/D_i = 44$

Gnielinski equation:

$$Nu = \frac{f/8(\mathrm{Re}-1000)\,\mathrm{Pr}}{1+12.7\sqrt{f/8}(\mathrm{Pr}^{2/3}-1)}\left[1+\left(\frac{D_i}{L}\right)^{2/3}\right] \tag{24}$$

Fig. 3 shows that the Nusselt number versus Reynolds number results have good agreements among the equations developed by Ghajar and Tam, Shah, and Gnielinski with the allowable deviation. The maximum dissimilarity of the experimental result was found with Eq. (20), which is approximately 10% in the turbulent flow region. This type of validation technique improves the confidence level in the measurement as well as the data reduction methodology.

3. Results and discussion

The local convective heat transfer coefficient as a function of axial distance for Fe_3O_4/DI-water nanofluids in laminar and turbulent flow regimes with different configurations of magnets across the height of the test section are shown in Figs. 4 and 5 respectively, with nanoparticle weight fractions 0.25 wt% and 0.50 wt%. Moreover, the convective heat transfer coefficients for both cases (case 1 and 2) is compared with the magnetite ferrofluid in the absence of a magnetic field.

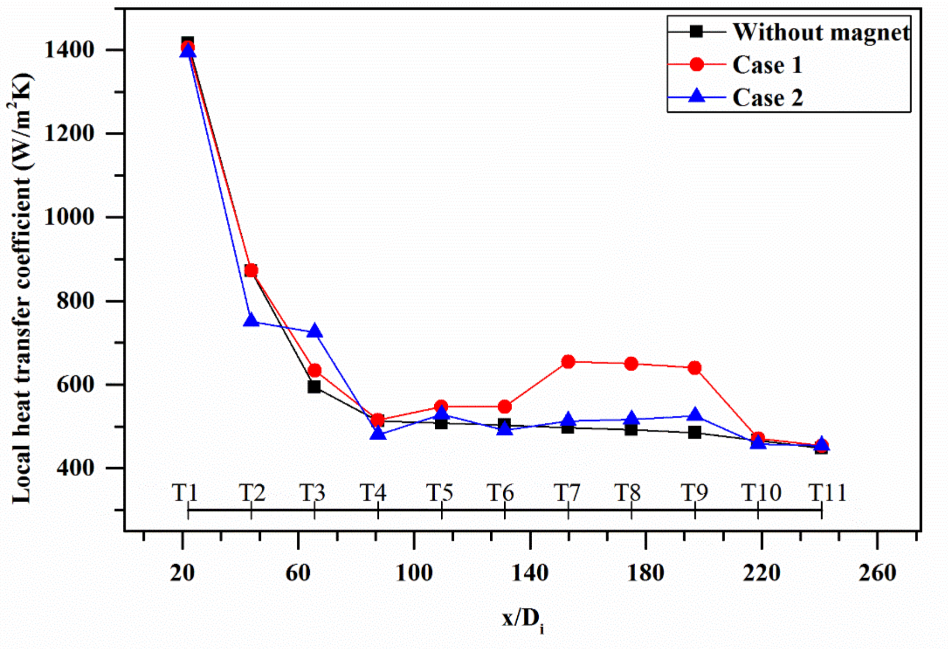

(a)

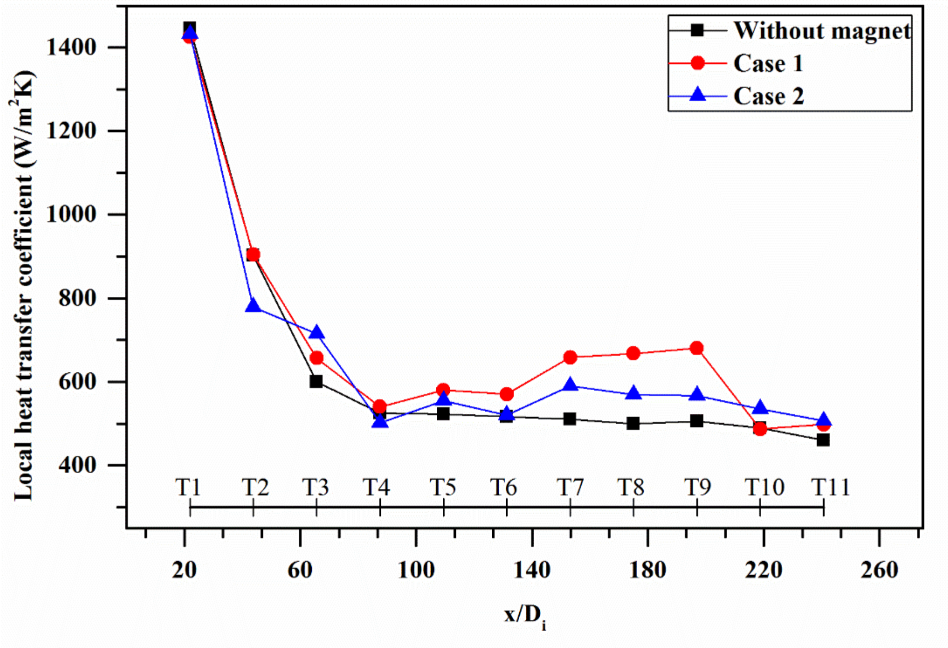

(b)

Fig 4. Local convective heat transfer coefficient of nanofluids along with axial position in laminar flow regime (Reynolds number = 715) (a) 0.25 wt% of Fe_3O_4/DI-water, (b) 0.50 wt% of Fe_3O_4/DI-water

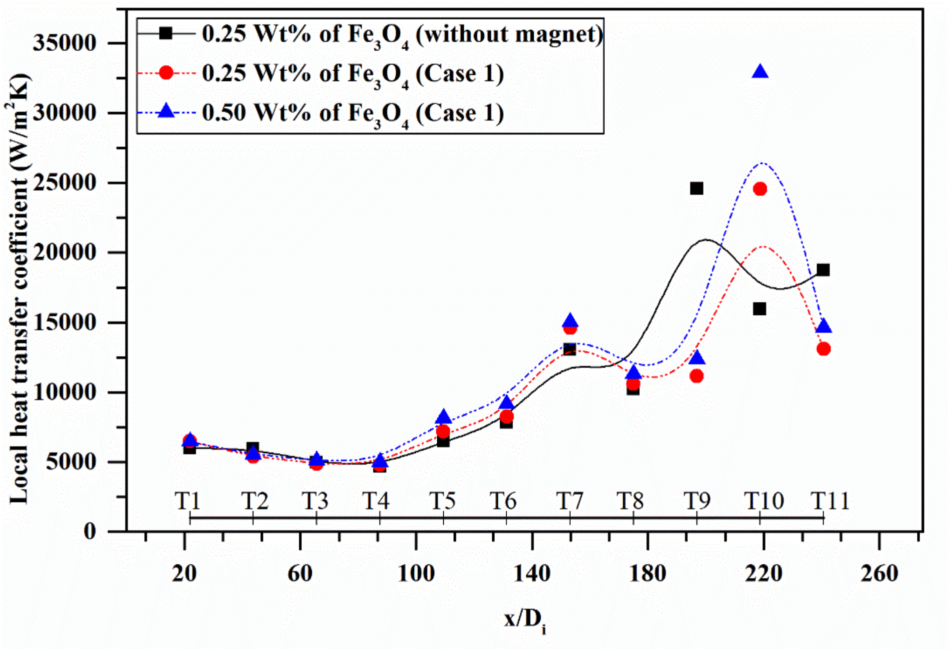

(a)

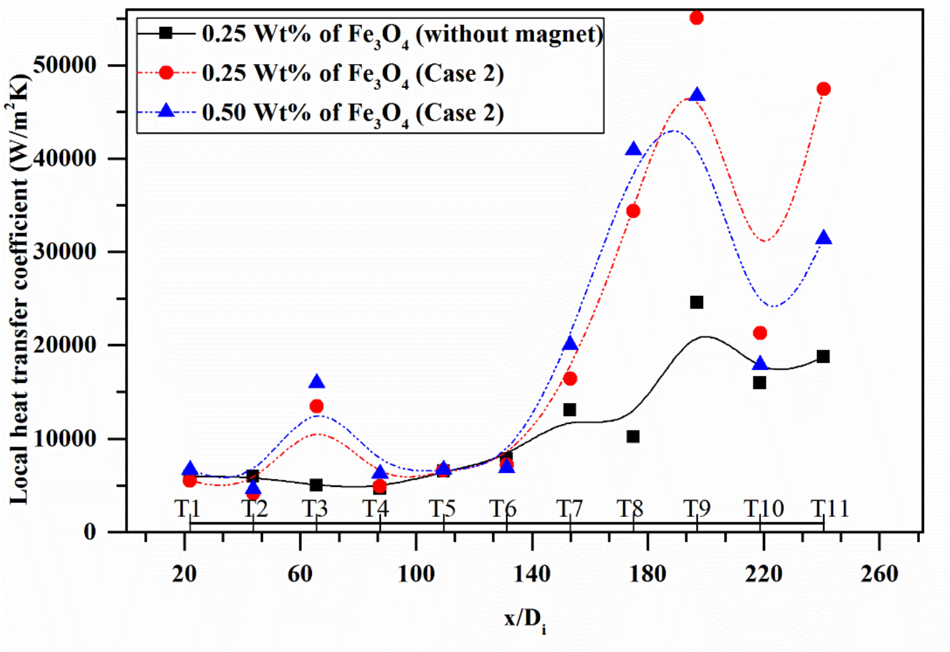

(b)

Fig 5. Local convective heat transfer coefficient of Fe_3O_4/DI-water nanofluids along with axial position in turbulent flow regime (Reynolds number = 2615) (a) case 1, (b) case 2

A significant increment in convective heat transfer coefficient was noticed in the existence of magnetic field due to the usage of permanent magnets. From the Figs. 4 and 5, the convective heat transfer coefficient attained highest value at T7–T9 thermocouple numbers in laminar flow and T7, T10 in turbulent flow regime for case 1, whereas the magnets were located (refer to Fig. 2). In addition, improvement in local heat transfer coefficient at the points T3, T7-T9 was found in laminar flow for case 2, and T8, T9, T11 represent the highest enhancement in heat transfer coefficient for turbulent flow region compare to the magnetite ferrofluid without any arrangement of magnet. Beyond these points, the heat transfer coefficient started to weaken at nearly the similar value as the magnetite nanofluids in the absence of magnetic field. Thermomagnetic convection effect may cause for the improvement of heat transfer coefficient of ferrofluids under the application of external magnets [20]. Nevertheless, a high temperature and large magnetic field gradients are required to get a thermomagnetic convection effect, and which is usually not considered as the forced convection situation. Most effective thermomagnetic convection will be found where natural convection could not supply sufficient heat transfer such as micro-electronic cooling.

Furthermore, the observed increase in convective heat transfer coefficient is expected to be related with the aggregation of Fe_3O_4/DI-water nanofluids toward the direction of magnetic field. The aggregation of nanoparticles initiate two different consequences. Firstly, it forms the low thermal resistance pathway for the heat transportation, consequently, the development of local thermal conductivity. Secondly, the interaction between the fluid flow and aggregates can enhance the local convective heat transfer coefficient. The aggregates improve the energy transfer and momentum, because it creates local obstructions, which is similar as a rough pipe, eventually rises the local convective heat transfer coefficient. It is very difficult to evaluate the relative influence of nanofluids' thermal conductivity over the local convective heat transfer coefficient enhancement experimentally. Because, in this study, the Nusselt number comprises the thermal conductivity of the nanofluid without the magnetic field, and hence in the absence of aggregation.

An improvement in the heat transfer coefficient was observed along the test section in the absence of magnetic field, particularly in turbulent flow condition (Fig. 5). This type of enhancement is associated with the probable changes in the flow pattern and the thermal boundary layer thickness due to the migration of the nanoparticles to the wall of the pipe in the presence of magnetic field and/or the kinetics of aggregation of the dispersion in the absence of magnetic field. The aggregate size decreases during the dispersion stage of the aggregation at a certain rate. The rate of dispersion is controlled by the flow conditions and surface force of the particles. As a result, the impact of enhancement continues while the aggregate size reduces or close to the primary size of the nanoparticles.

From Fig. 5, the convective heat transfer coefficient increases with the progression along the axial positon of the test section, which is on the contrary to the trend observed under laminar flow. Two different data trends were reported for the laminar and turbulent flow regimes, because two different mechanisms are apparent for heat transfer improvement in the two flow regimes [41]. The thermal entry length is defined as $x_{fd,t} \approx 0.05\,\mathrm{Re}_D \Pr D_i$ and $x_{fd,t} \approx 10D_i$ for laminar flow and turbulent flow condition, respectively [41]. Hence, there is a development in the thermal boundary layer across all of the axial positions under laminar flow, on the other hand, this development for turbulent flow was more than 10 times the axial length. Additionally, the observed fluctuation in heat transfer coefficient specially in turbulent flow regime can be described by the dynamics of the aggregate dispersion, growth and breakage. The variations possibly correspond with the formations of aggregates followed by breakages. The breakage occurs whenever the aggregates attain its maximum size. This process is followed by a development of primary particles in the fluid suspension which may join the broken aggregates.

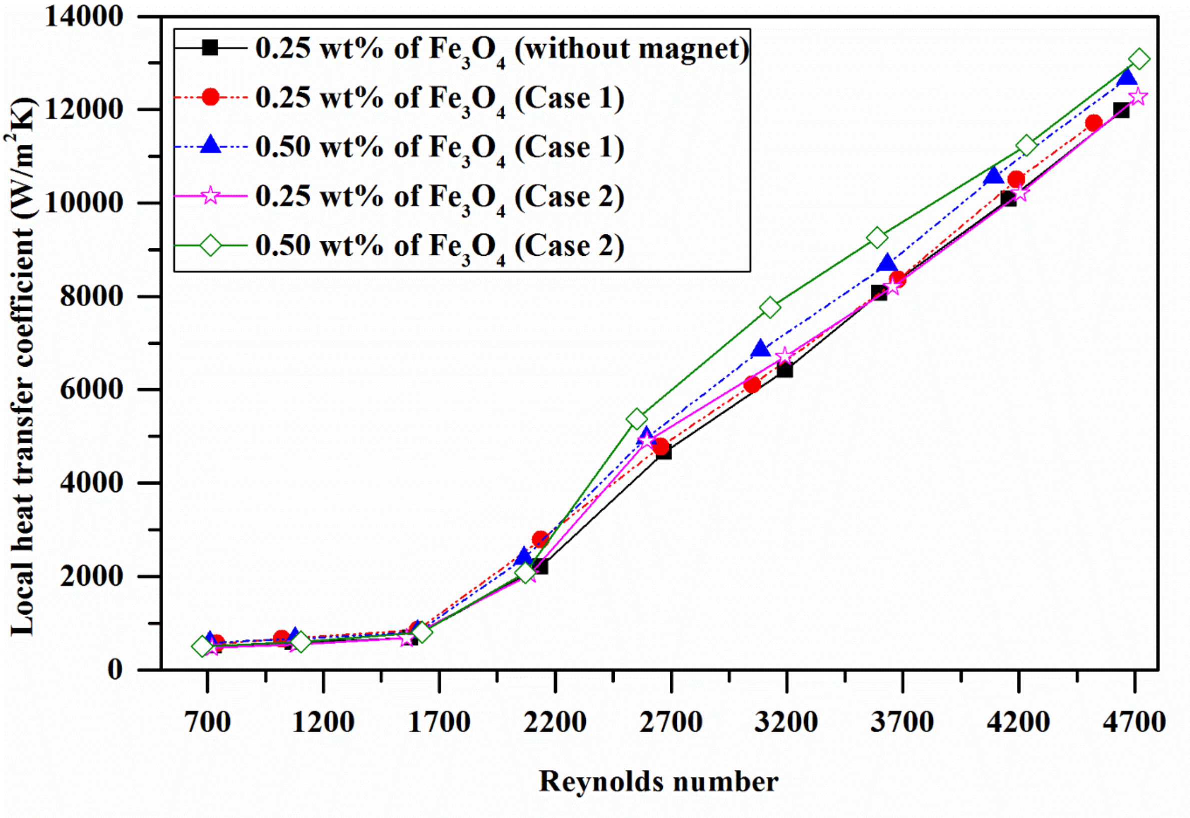

Fig 6. Convective heat transfer coefficient of Fe_3O_4/DI-water nanofluids as a function of Reynolds number in different configurations of magnets at x/D_i= 88.

Fig. 6 demonstrates the comparison of heat transfer coefficient of nanofluids at different weight fractions in the presence (case 1 and 2) and absence of external magnetic field. Under laminar flow conditions, the heat transfer coefficients for all nanofluids were almost same. This may be attributed to the fact that nanofluids exhibit shear thinning behaviour at low shear rates [42], which increases the viscosity and hence, reduce the value of heat transfer coefficient of the nanofluids. In turbulent flow regime, the highest enhancement in heat transfer coefficient was approximate 15% (on average) at 0.50 wt% of nanofluid in case 2 compare to nanofluids without magnets.

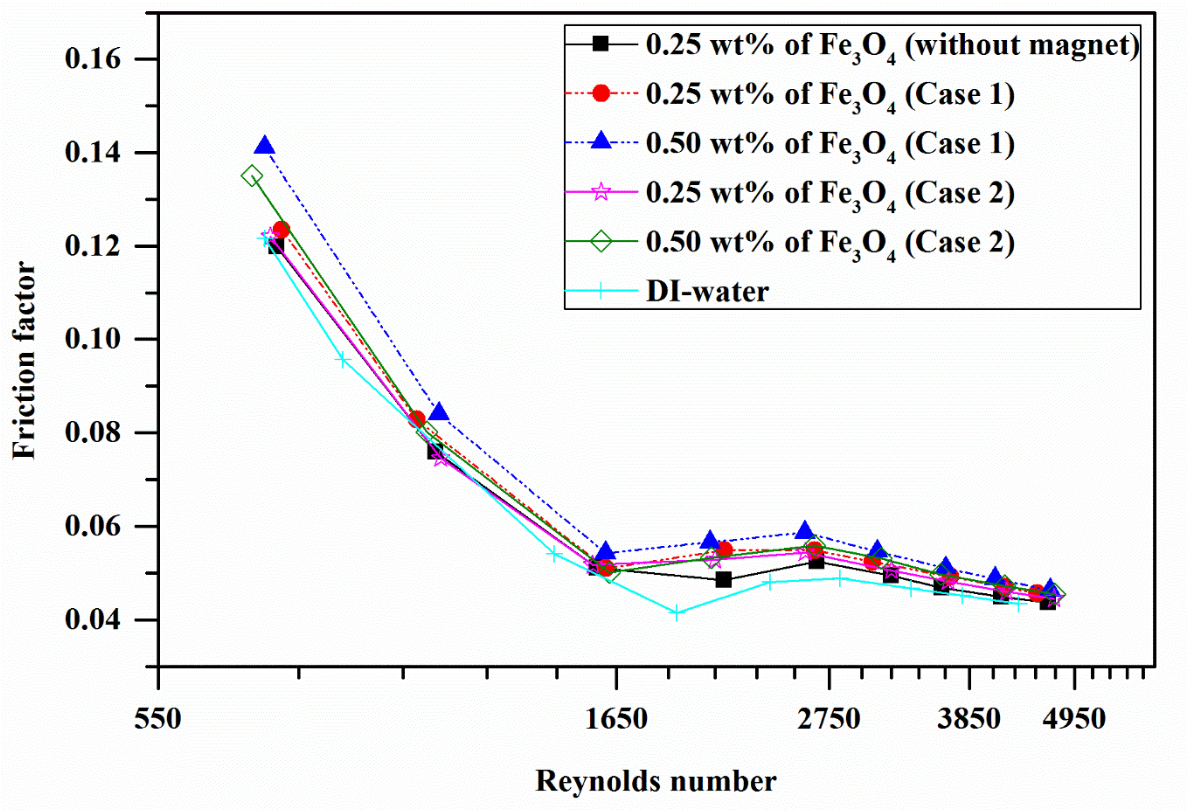

Fig. 7. Friction factor of different weight fraction of nanofluids as a function of Reynolds number in the presence and absence of magnetic fields.

A comparison of the friction factor for different weight concentrations of Fe_3O_4/DI-water nanofluids in both cases (case 1 and 2) for entire flow range was shown in Fig. 7. The results are compared with the same types of nanofluids without magnet. The average changeable friction factor value was around 6% in 0.50 wt% of magnetite ferrofluid for case 2 configuration. This result is very inspiring, because, a noticeable improvement in convective heat transfer coefficient (up-to 21%) is found with only a small rise in friction factor for the same class of nanofluid with same external magnets configuration. This may be due to the fact of more usage of magnets compare to case 1 arrangement. The friction factor enhancement in case 2 for both weight fractions (0.25 and 0.50 wt%) of ferrofluids is not much significant compare to the nanofluid without magnetic field. In addition, the friction factor of ferrofluids shows higher value compare to the friction factor of DI-water. The rise in nanofluids' friction factor may be related with an growth in nanoparticles weight fraction and aggregation which performs as roughness inside the tube in conjunction with magneto viscous effect due to the presence of an external magnetic field [43]. It is worth observing that without the direct measurement of particle size distribution in the flow channel, the assumption of nanoparticles aggregations and it consequences on pressure drop and heat transfer are rather questioning, but seems to be valid and reasonable.

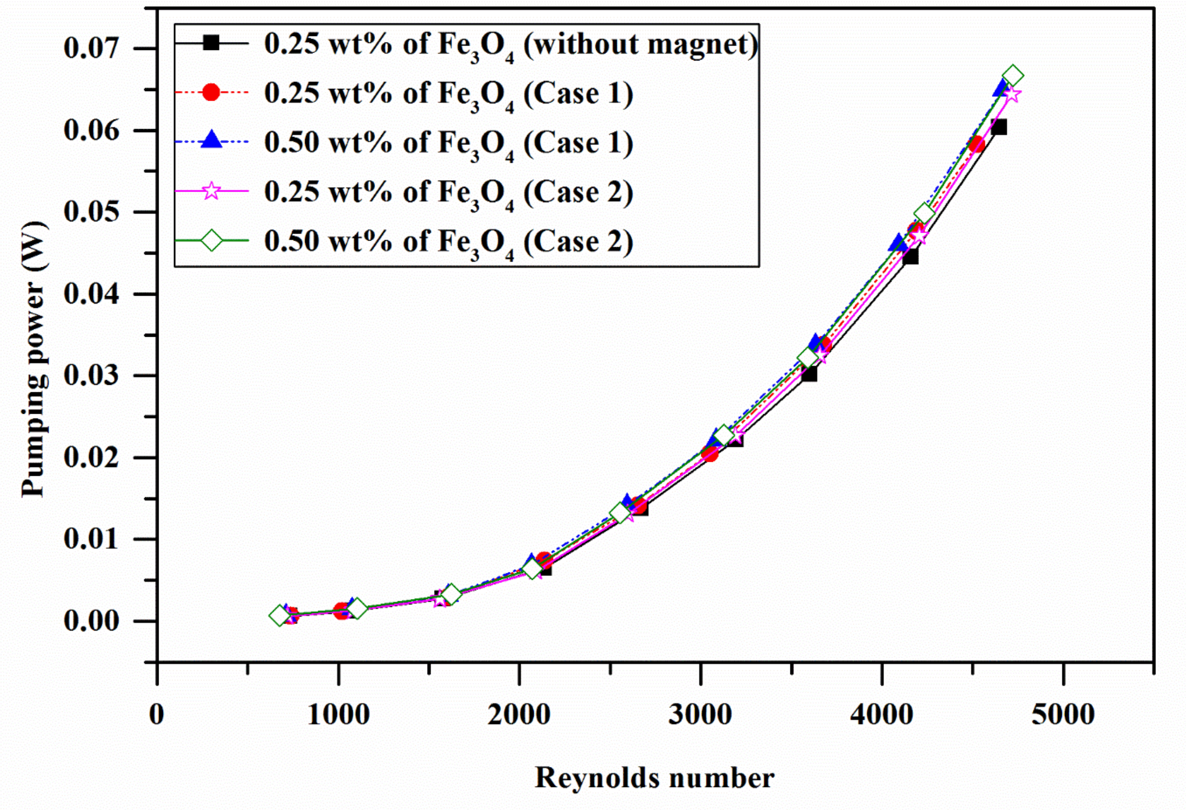

Fig. 8. Pumping power versus Reynolds number of Fe_3O_4/DI-water nanofluids for different magnet configurations

Fig. 8 shows the enhancement of pumping power as a function of Reynolds number. The pumping power was similar for all the nanofluids at the low Reynolds number, $Re < 2000$. As the Reynolds number increased above 2000, the pumping power of the nanofluids with high weight concentrations began to increase. Therefore, pumping power becomes more significant for higher mass flow rates, and as a result, it may influence the exergetic performance of the nanofluids [44]. Moreover, similar pumping power is found for both magnets arrangements at the same weight fraction of magnetite nanofluids. Pumping power is a function of the mass flow rate, density, and pressure drop (Eq. 14). Increases in pressure drop during the flow of the working fluid is an important parameter in determining the efficiency of nanofluids applications as the pressure drop and pumping power of the working fluid are closely related. There are a few properties which could influence pressure drop such as density and viscosity. It is expected that the pressure drop may increase with enhancements of the density and viscosity of the working fluid. This is one of the disadvantages for nanofluids applications as a cooling liquid. In the case of 0.25 wt% of nanofluids without magnet, there was a slight decrease in the pumping power in comparison to other magnetite nanofluids under magnetic field configurations. This may be attributed to the difference in viscosity and density of the nanofluids as well as the magnetic flux density. Hence, it was concluded that, nanofluids in the presence of magnets across the test section exhibit optimal heat transfer performance, with reasonable pumping power consumption.

Fig. 9 illustrates the exergy loss variation with nanoparticle weight concentration in the presence and absence of magnetic field. Case 2 exhibits the lowest exergy loss among the three cases in the laminar flow regime. The best exergetic utilisation of a thermal system is found when the entropy generation is a minimum [45]. At a greater usage of magnets, the entropy generation may decrease, and thus, comparatively an increase in exergy efficiency was observed for case 2 in both nanoparticle weight fractions.

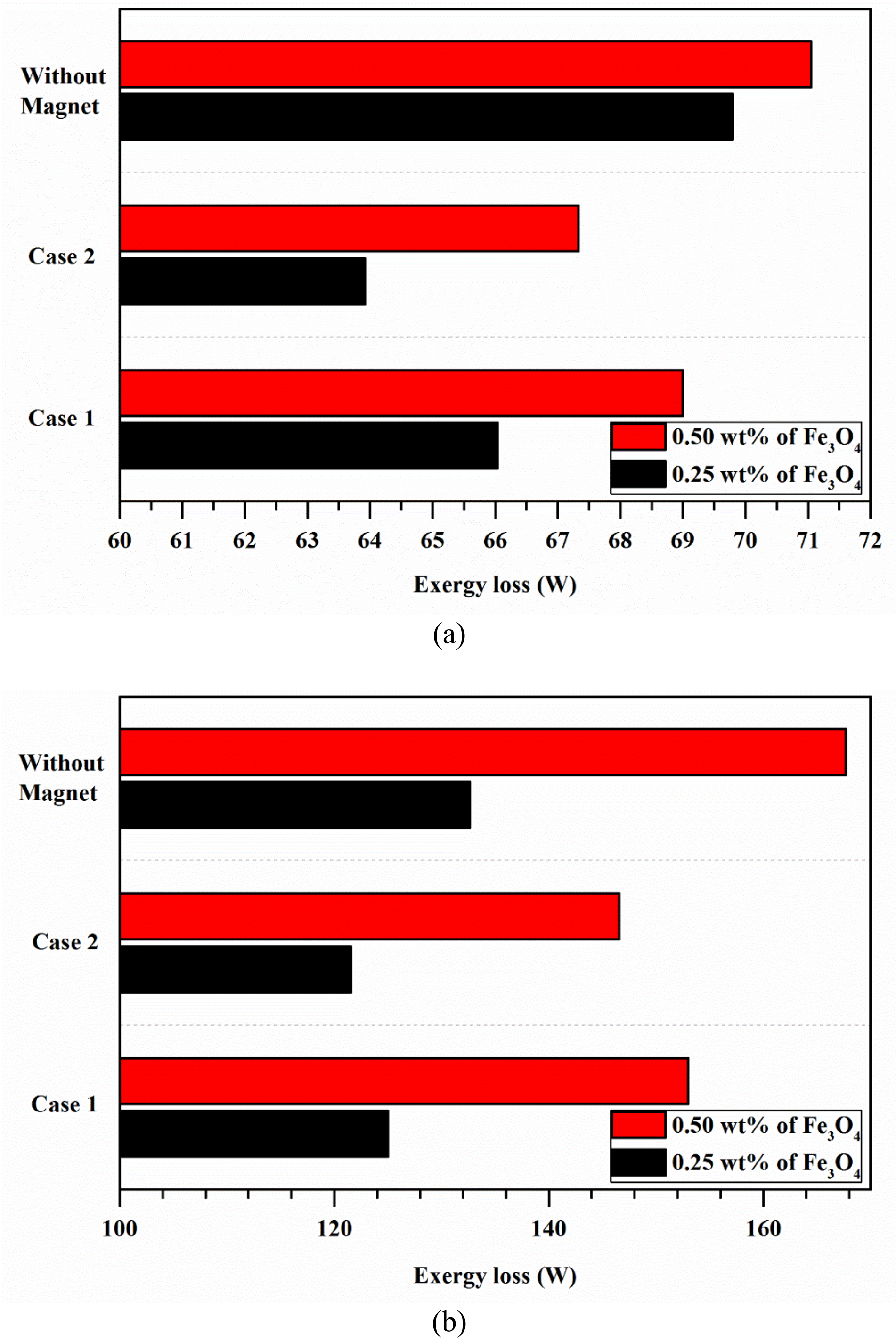

Fig. 9. Exergy loss of magnetite nanofluids with 0.25 wt% and 0.50 wt% at different external magnet configurations along the height of the test section (a) input power = 144 W, (b) input power = 282 W

Furthermore, exergy loss increases as the nanoparticle weight fraction is increased. It can be noted that the addition of nanoparticles to the base fluid leads to an enhancement of the effective heat transfer surface area. Therefore, in this study, the exergy loss was calculated using the Eq. (15), which is a function of specific heat capacity, mass flow rate, as well as inlet and outlet temperature of the working fluid. The specific heat capacity decreases with the increasing weight fraction of nanoparticles. In addition, the mass flow rate increases with increasing weight fraction of nanoparticles, because, it depends on the density of the working fluid. The increase in mass flow rate is was more significant than the reduction in the specific heat capacity of the nanofluids at greater weight concentrations; thus, the exergy loss was a minimum at the lowest weight fractions of nanoparticle. The above reasons may result in a reduction in the exergy loss while using nanofluids with lower weight fraction. This result agrees with Khaleduzzaman et al., and Pandey and Nema [44, 46].

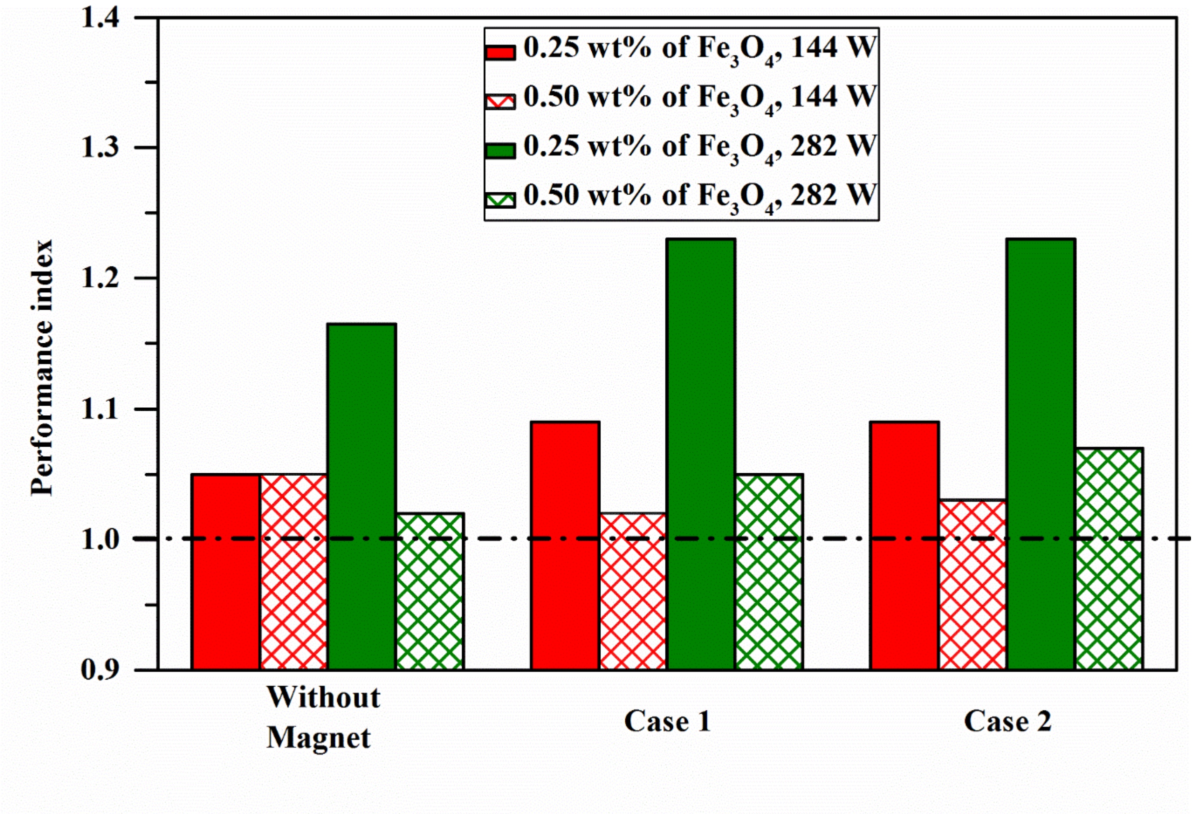

Fig. 10. Variation of efficiency index at different external magnets configurations as well as different input power for 0.25 wt% and 0.50 wt% of magnetite nanofluids

The performance index or efficiency index greater than one demonstrates that the application of nanofluids is more favourable in terms of improvement in heat transfer rather than the pressure drop enhancement. The term performance index helps to evaluate the ideal operating condition of an energy system by examining the simultaneous effects of the heat transfer and the pressure drop of the working fluids. Fig. 10 reveals the variation of the performance index of ferrofluids with different weight concentrations and arrangements of external magnets. The performance index of the Fe_3O_4/DI-water ferrofluids in all cases is greater than unity, therefore, the heat transfer enhancement dominates on increase in friction factor. The enhancement of the magnetite filed density by engaging more magnets has a positive impact on the efficiency index or performance factor. Moreover, the value of performance index decreases with the increment of ferrofluid weight concentrations. Hence, the magnetite nanofluids with higher concentrations may not be beneficial because of the excess pumping power requirement. A significant rise in η was found at higher input power. By changing the input power from lower to higher, the fluids temperature rises and consequently it changes the thermophysical properties of the nanofluids. Therefore, variations of such properties lead to deviate the amounts of friction factor as well as the Nusselt number.

4. Conclusion

The magnetite ferrofluids with two different nanoparticles weight concentrations were analysed under laminar and early turbulent flow regimes in the absence and presence of magnetic field. The improvement in the local heat transfer coefficient can be attained by placing the number of magnets across the test section, particularly in turbulent flow condition. The experimental results show an enhancement in the convective heat transfer coefficient at the positions between the ring magnets where the magnetic flux density is comparatively low compare to the surface of the magnets (i.e. T3, T7-T9 for case 2). This character specifies that the structures of aggregates stay unchanged over the distance between the two external magnets.

Moreover, this study also analysed the friction factor, pumping power, exergy loss and performance index to determine the potential thermal performance of nanofluids in a smooth stainless steel tube with vertical orientation under magnetic fields. From the result of the performance index of nanofluids, it is exposed that the usage of ferrofluids are far more advantageous (rising heat transfer) than their disadvantage (increasing friction factor). The results show that the magnetic field could not effect significantly to enhance the friction factor and pumping power. The rise in pumping power of 0.25 wt% of Fe_3O_4/DI-water nanofluids in the presence of magnets compare to the absence of the magnet are only 4.2% and 1.22% for case 1 and 2 magnet configurations, respectively. Furthermore, the nanofluids in case 2 magnet configuration could reduce a significant amount of exergy destruction compare to other arrangements.

It is concluded that in the presence of permanent magnets on the tube surface of the experimental test section demonstrate the highest performance index and heat transfer coefficient; and lowest friction factor and exergy loss. These characteristics make Fe_3O_4/DI-water nanofluids a potential and prominent candidate as a heat transfer fluids for thermal systems.

Acknowledgments

The authors gratefully acknowledge the financial support provided by the University of Newcastle (Australia), Granite Power Pty Ltd and the Australian Research Council through the

ARC-Linkage grant LP100200871, for the present study. The authors are thankful to Dr Ron Roberts for providing the technical supports and useful suggestions.

Appendix A.

Hall effect Gauss/Tesla meter

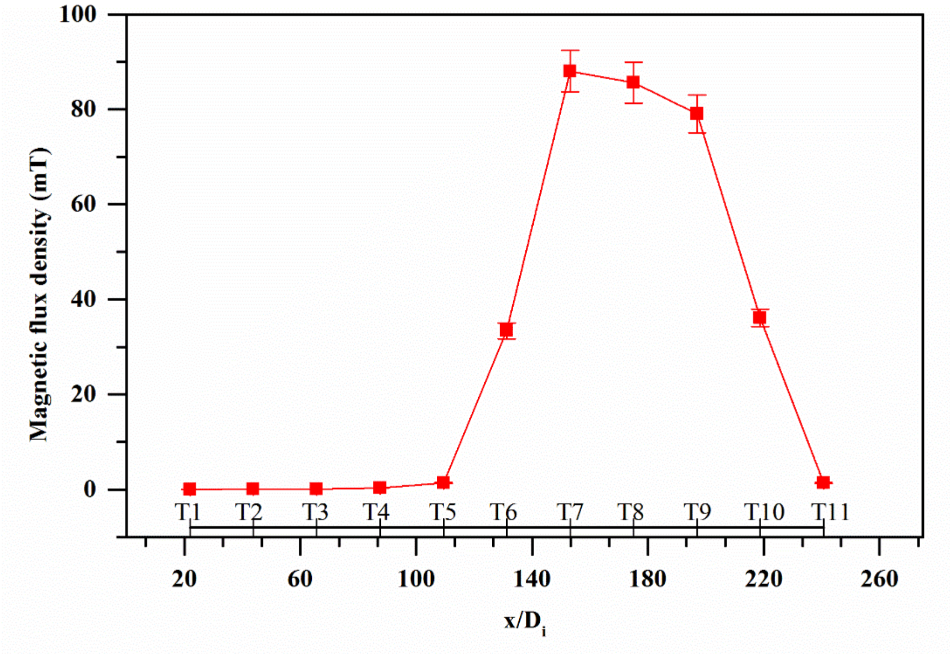

(a)

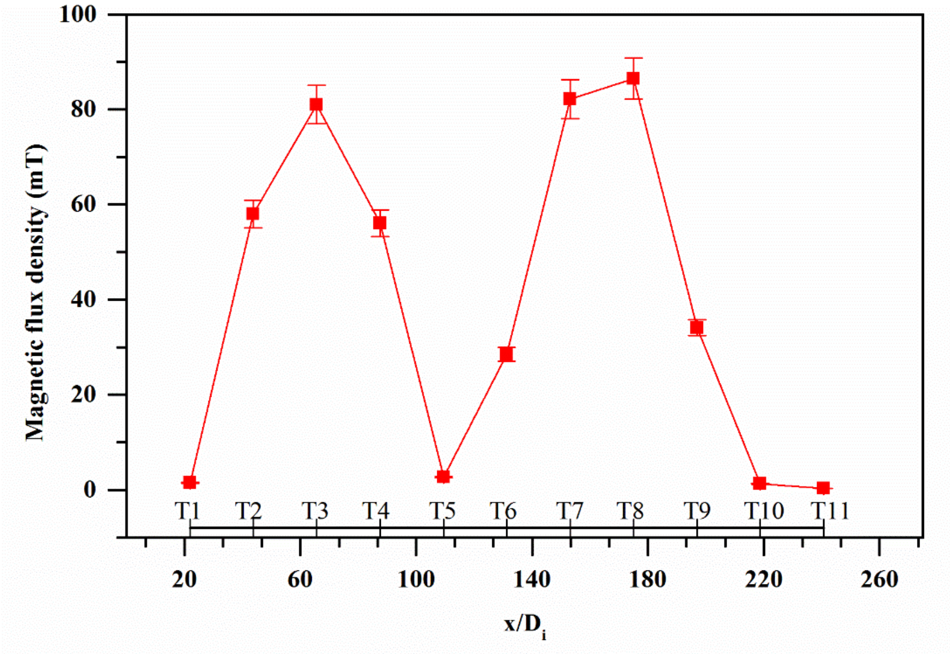

(b)

Fig. A1. Magnetic flux density along with axial position (a) case 1, (b) case 2

The 5180 Tesla meter is a magnetic measuring equipment manufactured by F.W. Bell was used in this study. This meter incorporates the use of digital signal processing technology and consists built-in software to eliminate the need for complex calibration procedures. Gauss meter operates based on Hall Effect in semiconductors. The magnetic field density on the surface of the tube was measured for both external magnets configurations (case 1 and 2). Fig. A1 shows the measurement result across the different positions of the test section.

Appendix B.

Thermocouple calibration procedure

The T-type thermocouples (range: -200*℃* to 350*℃*, uncertainty: 0.50 *℃*) do not need to be calibrated in the technical sense as this is done by NI-instrumentation with the reference of NIST calibration curves. However, all of the thirteen thermocouples were tested to confirm that there was no connection or manufacturing flaws, which may involve erroneous readings. The thermocouples were immersed in a well-maintained temperature bath at three different temperatures, 41°C, 58.5°C, 91.5°C, respectively. The results were the average of 300 data points, and shown in Table B1.

Table B1. Thermocouples testing result.

Avg. temperature (*℃*)	Min. temperature (*℃*)	Max. temperature (*℃*)	Standard deviation (*℃*)
40.91	40.71	41.16	0.12
58.54	58.06	58.97	0.27
91.77	90.94	92.63	0.50

It can be observed that the standard deviations are below or equal to the recommended uncertainty of the T-type thermocouples.

Appendix C.

Differential pressure transmitter calibration procedure

Regular calibration of the differential pressure transmitter was performed to ensure accurate pressure measurements. Firstly, a pressure transmitter as well as a digital calibration pressure gauge (accuracy: 0.05% FS, range: 0 to 103.4 kPa, Michigan, USA) were connected to a Dwyer low pressure calibration pump (output range: -40 to 40 kPa, Michigan, USA) with an adjusting resolution up to 0.01 Pa. Later, the pressure in the pressure pump was gradually increased for a range of pressure readings from 0 to 30 kPa. The pressure was recorded using a LabVIEW program, which output the reading of the pressure drop of the transmitter. Then, the value was compared with the reading of Dwyer digital calibration pressure gauge.

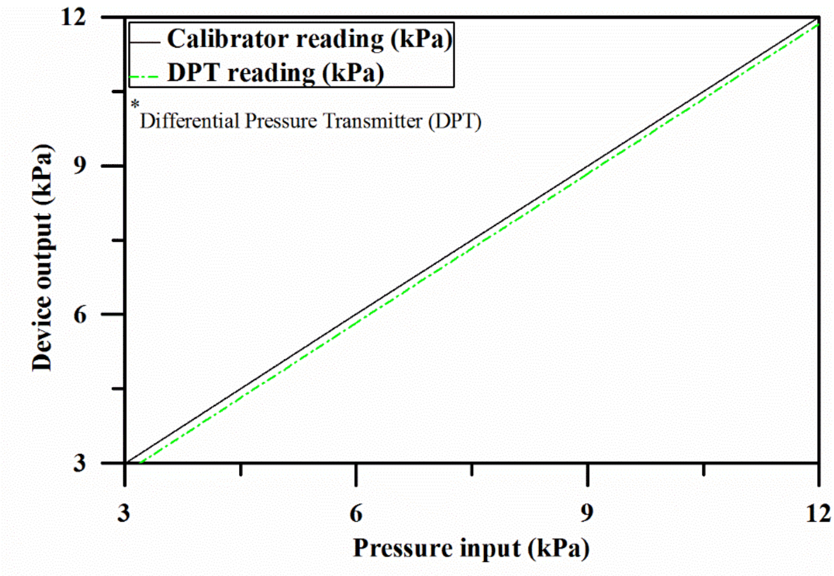

Fig. C1. Calibration curve of the differential pressure transmitter.

In this study, an offset trim was used without a slope trim to adjust the output of a transmitter to compensate for mounting position and line pressure effects. According to the supplier, typically, only an offset trim is required to adjust the calibration of a Rosemount Transmitter in the practical field. An offset trim is an adjustment that shifts the position of the sensor characterisation curve, but it does not affect the slope of the curve. This shift is illustrated in Fig. C1.

Appendix D.

Ultrasonic flow meter calibration procedure

Calibration of the ultrasonic flowmeter was conducted using simple techniques for flow meter calibration. The amount of fluid flow through the pipe of the test section was recorded with respect to time, and compared with the results recorded in the LabVIEW program that corresponds to the data point of volumetric flow rate of the working fluid through the test section. There was very favourable agreement with the manual and LabVIEW measurement data points shown in the Fig. D1.

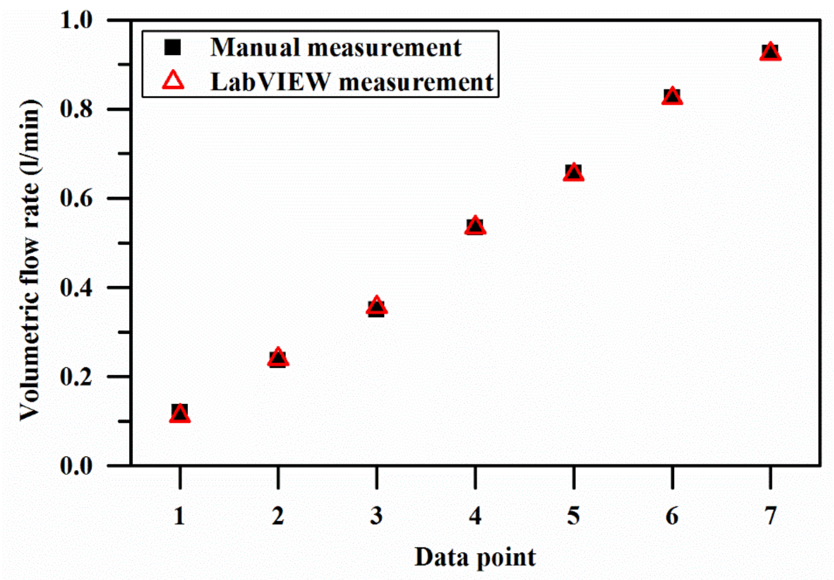

Fig. D1. Comparison of measurement of volumetric flow rate at different data points.

Appendix E.

Uncertainty analysis

In this study, error analysis has been completed using the procedure explained by Beckwith et al. [47]. Table E1 shows the vales of uncertainties from different instruments. The maximum possible error for the variables and parameters associated in this study are calculated using the following expressions, and summarised in Table E2.

Table E1. Uncertainties of instruments and properties

Variable	Uncertainty (%)
Wall temperature, $T_{w,i}$	0.435
Bulk temperature, T_b	0.627
Load regulation	0.5
Differential pressure transmitter	0.004
Ultrasonic flow meter	3
Thermophysical properties	0.1

(a) Heat flux,

$$q'' = \frac{\dot{m} c_p \Delta T}{\pi D_i L}$$

$$\frac{U_{q''}}{q''} = \sqrt{\left(\frac{U_{\dot{m}}}{\dot{m}}\right)^2 + \left(\frac{U_{cp}}{c_p}\right)^2 + \left(\frac{U_{\Delta T}}{\Delta T}\right)^2}$$

$$= \sqrt{(3)^2 + (0.1)^2 + (0.627)^2} = 3.07\%$$

(b) Reynolds number,

$$\mathrm{Re} = \frac{4\dot{m}}{\pi \mu D_i}$$

$$\frac{U_{\mathrm{Re}}}{\mathrm{Re}} = \sqrt{\left(\frac{U_{\dot{m}}}{\dot{m}}\right)^2 + \left(\frac{U_{\mu}}{\mu}\right)^2}$$

$$= \sqrt{(3)^2 + (0.1)^2} = 3\%$$

(c) Local heat transfer coefficient,

$$h_x = \frac{q''}{(T_{w,i} - T_b)_x}$$

$$\frac{U_{hx}}{h_x} = \sqrt{\left(\frac{U_{q''}}{q''}\right)^2 + \left(\frac{U_{(T_{w,i}-T_b)x}}{(T_{w,i} - T_b)_x}\right)^2}$$

$$= \sqrt{(3.07)^2 + (-0.192)^2} = 3.08\%$$

(d) Nusselt number,

$$Nu_x = \frac{h_x D_i}{k_x}$$

$$\frac{U_{Nu}}{Nu} = \sqrt{\left(\frac{U_{hx}}{h_x}\right)^2 + \left(\frac{U_{kx}}{k_x}\right)^2}$$

$$= \sqrt{(3.08)^2 + (0.1)^2} = 3.08\%$$

(e) Friction factor,

$$f = \frac{\Delta P.\rho.\pi^2.D_i^5}{8L.\dot{m}^2}$$

$$\frac{U_f}{f} = \sqrt{\left(\frac{U_{\Delta P}}{\Delta P}\right)^2 + \left(\frac{U_{\rho}}{\rho}\right)^2 + \left(\frac{U_{\dot{m}}}{\dot{m}}\right)^2}$$

$$= \sqrt{(0.004)^2 + (0.1)^2 + (3)^2} = 3\%$$

Table E2. Uncertainties of parameters and variables

Sl no.	Variable name	Uncertainty error (%)
(a)	Heat flux	3.07
(b)	Reynolds number	3
(c)	Local heat transfer coefficient	3.08
(d)	Nusselt number	3.08
(e)	Friction factor	3

References

[1] M. Bahiraei, M. Hangi, Flow and heat transfer characteristics of magnetic nanofluids: A review, Journal of Magnetism and Magnetic Materials, 374 (2015) 125-138.

[2] Y.-W. Lee, T.-L. Chang, Novel perturbations between magnetic nanofluid and the thermal fluidic system at heat dissipation, Microelectronic Engineering, 111 (2013) 58-63.

[3] Y. Iwamoto, H. Yamaguchi, X.-D. Niu, Magnetically-driven heat transport device using a binary temperature-sensitive magnetic fluid, Journal of Magnetism and Magnetic Materials, 323 (2011) 1378-1383.

[4] B. Wang, B. Wang, P. Wei, X. Wang, W. Lou, Controlled synthesis and size-dependent thermal conductivity of Fe_3O_4 magnetic nanofluids, Dalton Transactions, 41 (2012) 896-899.

[5] K. Parekh, H.S. Lee, Experimental investigation of thermal conductivity of magnetic nanofluids, AIP Conference Proceedings, 1447 (2012) 385-386.

[6] A. Gavili, F. Zabihi, T.D. Isfahani, J. Sabbaghzadeh, The thermal conductivity of water base ferrofluids under magnetic field, Experimental Thermal and Fluid Science, 41 (2012) 94-98.

[7] M. Bahiraei, M. Hangi, Automatic cooling by means of thermomagnetic phenomenon of magnetic nanofluid in a toroidal loop, Applied Thermal Engineering, 107 (2016) 700-708.

[8] S. Odenbach, S. Thurm, Magnetoviscous effects in ferrofluids, Springer, 2002.

[9] F. Fadaei, A. Molaei Dehkordi, M. Shahrokhi, Z. Abbasi, Convective-heat transfer of magnetic-sensitive nanofluids in the presence of rotating magnetic field, Applied Thermal Engineering, 116 (2017) 329-343.

[10] M. Lin, D. Zhang, J. Huang, J. Zhang, W. Xiao, H. Yu, L. Zhang, J. Ye, The anti-hepatoma effect of nanosized Mn–Zn ferrite magnetic fluid hyperthermia associated with radiation in vitro and in vivo, Nanotechnology, 24 (2013) 255101.

[11] A. Miaskowski, B. Sawicki, Magnetic Fluid Hyperthermia Modeling Based on Phantom Measurements and Realistic Breast Model, Biomedical Engineering, IEEE Transactions on, 60 (2013) 1806-1813.

[12] L. Syam Sundar, M.K. Singh, A.C.M. Sousa, Investigation of thermal conductivity and viscosity of Fe_3O_4 nanofluid for heat transfer applications, International Communications in Heat and Mass Transfer, 44 (2013) 7-14.

[13] Q. Li, Y. Xuan, J. Wang, Experimental investigations on transport properties of magnetic fluids, Experimental Thermal and Fluid Science, 30 (2005) 109-116.

[14] M.J. Pastoriza-Gallego, L. Lugo, J.L. Legido, M.M. Piñeiro, Enhancement of thermal conductivity and volumetric behavior of FexOy nanofluids, Journal of Applied Physics, 110 (2011) 014309.

[15] M. Abareshi, E.K. Goharshadi, S. Mojtaba Zebarjad, H. Khandan Fadafan, A. Youssefi, Fabrication, characterization and measurement of thermal conductivity of Fe_3O_4 nanofluids, Journal of Magnetism and Magnetic Materials, 322 (2010) 3895-3901.

[16] K.S. Hong, T.-K. Hong, H.-S. Yang, Thermal conductivity of Fe nanofluids depending on the cluster size of nanoparticles, Applied Physics Letters, 88 (2006) -.

[17] T.-H. Tsai, L.-S. Kuo, P.-H. Chen, C.-T. Yang, Effect of viscosity of base fluid on thermal conductivity of nanofluids, Applied Physics Letters, 93 (2008) 233121.

[18] M. Krichler, S. Odenbach, Thermal conductivity measurements on ferrofluids with special reference to measuring arrangement, Journal of Magnetism and Magnetic Materials, 326 (2013) 85-90.

[19] P.D. Shima, J. Philip, Tuning of Thermal Conductivity and Rheology of Nanofluids Using an External Stimulus, The Journal of Physical Chemistry C, 115 (2011) 20097-20104.

[20] M. Lajvardi, J. Moghimi-Rad, I. Hadi, A. Gavili, T. Dallali Isfahani, F. Zabihi, J. Sabbaghzadeh, Experimental investigation for enhanced ferrofluid heat transfer under magnetic field effect, Journal of Magnetism and Magnetic Materials, 322 (2010) 3508-3513.

[21] M. Goharkhah, M. Ashjaee, M. Shahabadi, Experimental investigation on convective heat transfer and hydrodynamic characteristics of magnetite nanofluid under the influence of an alternating magnetic field, International Journal of Thermal Sciences, 99 (2016) 113-124.

[22] M. Goharkhah, A. Salarian, M. Ashjaee, M. Shahabadi, Convective heat transfer characteristics of magnetite nanofluid under the influence of constant and alternating magnetic field, Powder Technology, 274 (2015) 258-267.

[23] R. Azizian, E. Doroodchi, T. McKrell, J. Buongiorno, L.W. Hu, B. Moghtaderi, Effect of magnetic field on laminar convective heat transfer of magnetite nanofluids, International Journal of Heat and Mass Transfer, 68 (2014) 94-109.

[24] L. Sha, Y. Ju, H. Zhang, J. Wang, Experimental investigation on the convective heat transfer of Fe_3O_4/water nanofluids under constant magnetic field, Applied Thermal Engineering, 113 (2017) 566-574.

[25] E. Esmaeili, R. Ghazanfar Chaydareh, S.A. Rounaghi, The influence of the alternating magnetic field on the convective heat transfer properties of Fe_3O_4-containing nanofluids through the Neel and Brownian mechanisms, Applied Thermal Engineering, 110 (2017) 1212-1219.

[26] M.A. Rosen, I. Dincer, M. Kanoglu, Role of exergy in increasing efficiency and sustainability and reducing environmental impact, Energy Policy, 36 (2008) 128-137.

[27] E. Shojaeizadeh, F. Veysi, Development of a correlation for parameter controlling using exergy efficiency optimization of an Al_2O_3/water nanofluid based flat-plate solar collector, Applied Thermal Engineering, 98 (2016) 1116-1129.

[28] M.A. Khairul, E. Doroodchi, R. Azizian, B. Moghtaderi, Experimental Study on Fundamental Mechanisms of Ferro-Fluidics for an Electromagnetic Energy Harvester, Industrial & Engineering Chemistry Research, 55 (2016) 12491-12501.

[29] M.A. Khairul, M.A. Alim, I.M. Mahbubul, R. Saidur, A. Hepbasli, A. Hossain, Heat transfer performance and exergy analyses of a corrugated plate heat exchanger using metal oxide nanofluids, International Communications in Heat and Mass Transfer, 50 (2014) 8-14.

[30] W. Yu, S.U.S. Choi, The Role of Interfacial Layers in the Enhanced Thermal Conductivity of Nanofluids: A Renovated Maxwell Model, Journal of Nanoparticle Research, 5 (2003) 167-171.

[31] K.H. Solangi, S.N. Kazi, M.R. Luhur, A. Badarudin, A. Amiri, R. Sadri, M.N.M. Zubir, S. Gharehkhani, K.H. Teng, A comprehensive review of thermo-physical properties and convective heat transfer to nanofluids, Energy, 89 (2015) 1065-1086.

[32] M.A. Khairul, E. Doroodchi, R. Azizian, B. Moghtaderi, The influence of different flow regimes on heat transfer performance and exergy loss of Al_2O_3/DI-water and CuO/DI-water nanofluids, Applied Thermal Engineering, 122 (2017) 566-578.

[33] A. International, P.J. Blau, J.R. Davis, ASM Handbook: Properties and Selection: Irons, Steels, and High-performance Alloys, ASM International, 2001.

[34] M. Voldsund, T.-V. Nguyen, B. Elmegaard, I.S. Ertesvåg, A. Røsjorde, K. Jøssang, S. Kjelstrup, Exergy destruction and losses on four North Sea offshore platforms: A comparative study of the oil and gas processing plants, Energy, 74 (2014) 45-58.

[35] S. Zimmermann, M.K. Tiwari, I. Meijer, S. Paredes, B. Michel, D. Poulikakos, Hot water cooled electronics: Exergy analysis and waste heat reuse feasibility, International Journal of Heat and Mass Transfer, 55 (2012) 6391-6399.

[36] J.A.W. Gut, R. Fernandes, J.M. Pinto, C.C. Tadini, Thermal model validation of plate heat exchangers with generalized configurations, Chemical Engineering Science, 59 (2004) 4591-4600.

[37] M.A. Akhavan-Behabadi, F. Hekmatipour, S.M. Mirhabibi, B. Sajadi, Experimental investigation of thermal–rheological properties and heat transfer behavior of the heat transfer oil–copper oxide (HTO–CuO) nanofluid in smooth tubes, Experimental Thermal and Fluid Science, 68 (2015) 681-688.

[38] A.J. Ghajar, L.-M. Tam, Heat transfer measurements and correlations in the transition region for a circular tube with three different inlet configurations, Experimental Thermal and Fluid Science, 8 (1994) 79-90.

[39] L.J.H.V. Lienhard J.H. IV, A Heat Transfer Textbook, Second ed., Phlogiston Press, 2002.

[40] V. Gnielinski, New equations for heat and mass-transfer in turbulent pipe and channel flow, International chemical engineering, 16 (1976) 359-368.

[41] D. Kim, Y. Kwon, Y. Cho, C. Li, S. Cheong, Y. Hwang, J. Lee, D. Hong, S. Moon, Convective heat transfer characteristics of nanofluids under laminar and turbulent flow conditions, Current Applied Physics, 9 (2009) e119-e123.

[42] M.A. Khairul, K. Shah, E. Doroodchi, R. Azizian, B. Moghtaderi, Effects of surfactant on stability and thermo-physical properties of metal oxide nanofluids, International Journal of Heat and Mass Transfer, 98 (2016) 778-787.

[43] N. Andhariya, B. Chudasama, R. Patel, R.V. Upadhyay, R.V. Mehta, Field induced rotational viscosity of ferrofluid: Effect of capillary size and magnetic field direction, Journal of Colloid and Interface Science, 323 (2008) 153-157.

[44] S.S. Khaleduzzaman, R. Saidur, I.M. Mahbubul, T.A. Ward, M.R. Sohel, I.M. Shahrul, J. Selvaraj, M.M. Rahman, Energy, Exergy, and Friction Factor Analysis of Nanofluid as a Coolant for Electronics, Industrial & Engineering Chemistry Research, 53 (2014) 10512-10518.

[45] M. Moghaddami, A. Mohammadzade, S.A.V. Esfehani, Second law analysis of nanofluid flow, Energy Conversion and Management, 52 (2011) 1397-1405.

[46] S.D. Pandey, V.K. Nema, Experimental analysis of heat transfer and friction factor of nanofluid as a coolant in a corrugated plate heat exchanger, Experimental Thermal and Fluid Science, 38 (2012) 248-256.

[47] T.G. Beckwith, R.D. Marangoni, J.H. Lienhard, Mechanical measurements, 5th ed., Addison-Wesley Publishing Company, New York, 1990.